Spontaneous Gap Opening and Potential Excitonic States in an Ideal Dirac Semimetal $Ta_2Pd_3Te_5$

Peng Zhang,[1,2,*,†] Yuyang Dong,[3,*] Dayu Yan,[4,5,*] Bei Jiang,[4,5,*] Tao Yang,[1] Jun Li,[4] Zhaopeng Guo,[4,5] Yong Huang,[1] Haobo,[6] Qing Li,[1] Yupeng Li,[4] Kifu Kurokawa,[3] Rui Wang,[1,2] Yuefeng Nie,[6] Makoto Hashimoto,[7] Donghui Lu,[7] Wen-He Jiao,[8] Jie Shen,[4] Tian Qian,[4,5] Zhijun Wang,[4,5] Youguo Shi,[4,5] and Takeshi Kondo[3,9,‡]

[1]*School of Physics and National Laboratory of Solid State Microstructures,*
Nanjing University, Nanjing, China
[2]*Collaborative Innovation Center for Advanced Microstructures, Nanjing, China*
[3]*Institute for Solid State Physics, the University of Tokyo, Kashiwa, Chiba 277-8581, Japan*
[4]*Beijing National Laboratory for Condensed Matter Physics, Institute of Physics,*
Chinese Academy of Sciences, Beijing, China
[5]*University of Chinese Academy of Sciences, Beijing, China*
[6]*National Laboratory of Solid State Microstructures, Jiangsu Key Laboratory of Artificial Functional*
Materials, College of Engineering and Applied Sciences, Nanjing University, Nanjing, China
[7]*Stanford Synchrotron Radiation Lightsource, SLAC National Accelerator Laboratory,*
Menlo Park, California, USA
[8]*Key Laboratory of Quantum Precision Measurement of Zhejiang Province,*
Department of Applied Physics, Zhejiang University of Technology, Hangzhou, China
[9]*Trans-scale Quantum Science Institute, The University of Tokyo, Tokyo 113-0033, Japan*

(Received 6 December 2022; revised 21 December 2023; accepted 1 February 2024; published 13 March 2024)

The opening of an energy gap in the electronic structure generally indicates the presence of interactions. In materials with low carrier density and short screening length, long-range Coulomb interaction favors the spontaneous formation of electron-hole pairs, so called excitons, opening an excitonic gap at the Fermi level. Excitonic materials host unique phenomena associated with pair excitations. However, there is still no generally recognized single-crystal material with excitonic order, which is, therefore, awaited in condensed matter physics. Here, we show that excitonic states may exist in the quasi-one-dimensional material $Ta_2Pd_3Te_5$, which has an almost ideal Dirac-like band structure, with the Dirac point located exactly at the Fermi level. We find that an energy gap appears at 350 K, and it grows with decreasing temperature. The spontaneous gap opening is absent in a similar material $Ta_2Ni_3Te_5$. Intriguingly, the gap is destroyed by the potassium deposition on the crystal, likely due to extra-doped carriers. Furthermore, we observe a pair of in-gap flat bands, which is an analog of the impurity states in a superconducting gap. All these observations can be properly explained by an excitonic order, providing $Ta_2Pd_3Te_5$ as a new and promising candidate realizing excitonic states.

DOI: 10.1103/PhysRevX.14.011047

Subject Areas: Condensed Matter Physics,
Materials Science

When the dimensionality is reduced, the screening of the Coulomb interaction becomes weak, leading to strong electron correlations in favor of various novel states. One such example is an excitonic state, which hosts electron-hole pairs bounded by Coulomb attraction, namely, the excitons. The excitonic order builds up spontaneously when the binding energy of excitons is larger than the original band gap [1]. Similar to superconductors, excitonic insulators open an energy gap corresponding to the binding energy of excitons and have a pair-breaking effect by impurity scattering [2]. In contrast to a large variety of superconducting materials, however, excitonic insulator candidates are very rare.

Excitonic states have been so far reported for some fabricated bilayer structures [3–8] and for monolayer tellurides [9–12]. There are also reports for single crystals but only of two compounds under normal conditions: $1T$-$TiSe_2$ and Ta_2NiSe_5 [13–21]. These two single-crystal candidates, however, entangle with other phase transitions, making the verification of the possible excitonic states

---

[*] These authors contributed equally to this work.

[†] zhangpeng@nju.edu.cn

[‡] kondo1215@issp.u-tokyo.ac.jp

rather complex. In $1T$-TiSe$_2$, the valence and conduction bands are located at different momentum spaces with an indirect gap. The excitonic pairing with a finite wave vector naturally coexists with a charge-density wave (CDW), leading to intrinsic difficulties in distinguishing excitonic order from a CDW. In Ta$_2$NiSe$_5$, both the valence band and conduction band locate at the Brillouin zone center with a direct gap. In such a case, there is no coexisting CDW. However, an orthorhombic-to-monoclinic structure transition appears at the proposed excitonic transition temperature. Whether the change of energy gap is induced by excitonic order or structure transition, is still under debate [22–24]. Because of these circumstances, one has been waiting for single crystals which host only excitonic order and do not entangle with other phase transitions. In particular, theoretical calculations [25] predict the Ta$_2$Pd$_3$Te$_5$ monolayer to be an excitonic insulator with rather simple band structures, inspiring experiments to explore the possible excitonic states in the single crystals of this compound.

An ideal Dirac semimetal, in which the Dirac point is located exactly at the Fermi level, has very low carrier density (almost zero), and the electron and hole excitations are almost symmetric. In such a unique system, it is expected that the electrons and holes are easily bounded by Coulomb interaction, and an excitonic order naturally occurs. In this work, we find such an ideal Dirac semimetal state in single-crystal material Ta$_2$Pd$_3$Te$_5$, with the following features supporting the existence of excitonic order: (i) There is an energy gap opening at 350 K, and it is associated with a tiny lattice distortion unveiled by electron diffraction. (ii) The spontaneous gap opening is absent in a similar material Ta$_2$Ni$_3$Te$_5$. (iii) The energy gap is destroyed by carrier doping, according to our experiments of the potassium deposition on the crystal surface. (iv) The in-gap spectra show double flat dispersions in the energy gap, most likely from impurity states, similar to those emerging in superconductors due to the breaking of Cooper pairs [26,27]. These observations put a strong limitation on the origin of the energy gap and are, most importantly, explained reasonably by an excitonic order.

Ta$_2$Pd$_3$Te$_5$ single crystals are synthesized by the self-flux method. Details of the synthesis process can be found in Ref. [28]. The high-resolution angle-resolved photoemission spectroscopy (ARPES) measurements are carried out with a 6.994-eV laser and a VG-Scienta R4000WAL electron analyzer at the Institute for Solid State Physics, The University of Tokyo. The energy resolution for the experiments is set to approximately 3 meV. The synchrotron ARPES measurements are performed at beamline 5-2 of the Stanford Synchrotron Radiation Lightsource with a ScientaOmicron DA30L analyzer. The overall energy resolution is 10–20 meV. In both ARPES experiments, the spot size of incident light is smaller than approximately 50 μm. The samples are cleaved *in situ* and kept in an ultrahigh vacuum below 5×10^{-11} Torr during the ARPES measurements.

Ta$_2$Pd$_3$Te$_5$ has a quasi-1D crystal structure [28–31], with Ta-Te or Pd-Te chains along the b axis [Fig. 1(a)]. The resistivity measurement [Fig. 1(b)] shows a typical semiconducting behavior at low temperatures. It shows an upturn around 350–360 K and becomes metalliclike above 350–360 K, indicating some changes in the electronic structure. Indeed, electron-diffraction experiments unveil some structure distortions. As shown in Fig. 1(c), at 370 K the electron-diffraction data taken along the [001] zone axis consist of diffraction peaks with $k + l = 2n$ (hkl are Miller indices, and n is an integer), consistent with that of space group no. 62, while at 94 K the peaks with $k + l = 2n + 1$ appear. From the temperature evolution in Fig. 1(d), we find the distortion happens around 330 K [thick line in Fig. 1(d)], roughly consistent with the transition temperature in resistivity measurement. We note the emerged $k + l = 2n + 1$ peaks at 94 K are very weak. For example, the (005) peak intensity is just 2.7% of the (004) peak intensity in Fig. 1(c). This indicates a very small lattice distortion. Indeed, x-ray diffraction (XRD) along (h00) and specific heat measurement did not resolve such a small structure distortion (Supplemental Material [32] Fig. 2), probably because they are not as efficient as electron diffraction. More sophisticated measurements may be able to resolve this tiny lattice distortion from XRD and specific heat.

In Fig. 1(e), we plot the ARPES intensity map measured at 10 K along the Γ-Y-Z sheet slightly below the Fermi level (E_F) at -30 meV. The quasi-1D character of the electronic structure is evident from parallel segments with only a little warping. This feature is more clearly demonstrated in the right inset panel by taking the curvature of the ARPES intensities to show the location of energy states [33]. Figures 1(f) and 1(g) display the band structures along the high-symmetry lines Γ-Z and Γ-Y described as cut 1 and cut 2 in Fig. 1(e), respectively. The energy dispersion is much stronger along cut 2 than along cut 1 due to the quasi-1D structure. Along cut 2, we observe three humps just below E_F, consisting of an m-shaped band and an n-shaped band in the middle, as illustrated in Fig. 1(g).

We investigate the evolution of the band structure over a wide range of temperatures from 350 to 20 K, with 30- and 67-eV photons, as displayed in Figs. 2(a) and 2(b). Here the data are divided by the Fermi function at measurement temperatures to remove the cutoff effect above E_F. At 350 K [Figs. 2(a2) and 2(b2)], Dirac-type bands are observed. It is further clarified in Figs. 2(a1) and 2(b1) by taking the curvature of Figs. 2(a2) and 2(b2). The Dirac point is located almost exactly at the Fermi level, indicating an ideal Dirac semimetal state. The band dispersions at different photon energies are extracted and illustrated in Fig. 2(c). Except for one m-shaped valence band and one cone-shaped (n shaped at low temperatures) valence band, the conduction bands from 30- and 67-eV data show

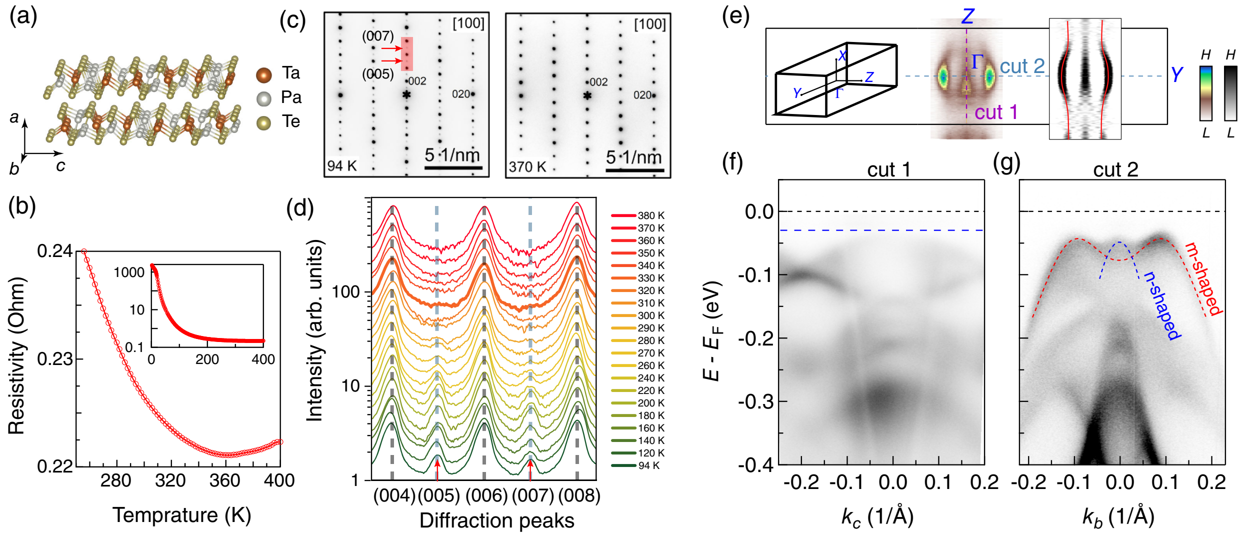

FIG. 1. The crystal structure and electronic properties of $Ta_2Pd_3Te_5$. (a) Crystal structure of $Ta_2Pd_3Te_5$. The Ta-Te chains are along the b axis. (b) Resistivity curve from 250 to 400 K. The inset shows the overall behavior from 2 to 400 K. (c) Electron-diffraction measurement of the [100] zone axis. The data are taken at 94 and 370 K, respectively. (d) Temperature evolution of the (00l) peaks. The vertical intensity axis is in a log scale. See Supplemental Material [32] Fig. 1 for the same plot in a linear scale. (e) Intensity mapping in k space around the Γ-Z line measured by a 7-eV laser ARPES. The data are taken at −30 meV [dashed blue line in (f)] and integrated over an energy window of ±5 meV. The left and right insets show the bulk Brillouin zone and the curvature plot of the data in gray scale, respectively. (f),(g) Band structures measured at 10 K by ARPES, perpendicular to the chain [cut 1 in (e)] with s-polarized light and along the chain [cut 2 in (e)] with p-polarized light, respectively.

slightly different dispersions. These two dispersions may come either from the same band at different k_a (out-of-plane direction, or k_z in general expression for ARPES) or different bands. We cannot distinguish between these two scenarios due to the limited momentum resolution along k_a in ARPES. The first-principles calculations (Supplemental Material [32] Fig. 3) show only one conduction band with a small k_a dispersion around E_F; this suggests that conduction bands of the 30- and 67-eV data are likely originated from the same band and exhibit slightly different dispersions due to different k_a.

Since the m-shaped valence band does not cross E_F, we focus on the cone-shaped (n shaped at low temperatures) valence band and the conduction band crossing E_F. With decreasing temperature, an energy gap gradually develops between the conduction and valence bands in both Figs. 2(a2)–2(a6) and 2(b2)–2(b6). The gap-opening feature is further demonstrated in Fig. 2(d) by plotting the intensity difference between the data at 250 and 350 K for 30 eV. The reduced intensity (blue color) due to a gap opening (Δ) is seen around E_F. We note the intensities just below E_F in Figs. 2(a6) and 2(b6) are from impurity states (ISs), which are discussed in detail in Fig. 5.

We examine the gap behavior in more detail by tracing the temperature evolution of the valence-band top (E_v) and the conduction-band bottom (E_c). We trace E_v from 30-eV data and E_c from 30- and 67-eV data [see cyan, red, and blue arrows in Figs. 2(a3), 2(a5), and 2(b3), respectively]. The E_v is obtained from the curvature-enhanced intensity plot in Fig. 2(e), which corresponds to the dashed box region in Fig. 2(a5). We see the shifting down of E_v from −27 meV at 200 K to −54 meV at 20 K. Above 200 K, however, the valence-band top has some intensity overlap with the conduction-band bottom, so the E_v cannot be accurately determined. The temperature evolution of E_v from 30-eV data is plotted with a solid red line in Fig. 2(g) for the range below 200 K. We determine the E_c at 67 eV directly from the peak positions of the energy distribution curves (EDCs), as shown in Fig. 2(f) with blue dots marking the peaks. The evolution of E_c from 67-eV data with the temperature is plotted with a solid blue line in Fig. 2(g). The cyan E_c curve is acquired in a similar way, but from 30-eV data. Note that the plot is only for the range above 150 K, since the band bottom cannot be reliably extracted below 150 K due to the cutoff effect of the Fermi function.

Both E_c and E_v values are acquired at 150 and 200 K and they are roughly equal. Thus, it would be reasonable to assume that the band gap opens symmetrically to E_F, $E_c \approx E_v$. With this assumption, we can compensate the missing values of E_c and E_v at low and high temperatures, respectively, by mirroring the solid red and blue lines according to E_F, as shown in Fig. 2(g). The difference between the mirrored and original curves in the overlapped temperature range (150 and 200 K) is small enough to justify the assumption of symmetric gap opening to E_F. The dashed black lines sketch the full evolution of the conduction and valence bands, and thus, the gap with the

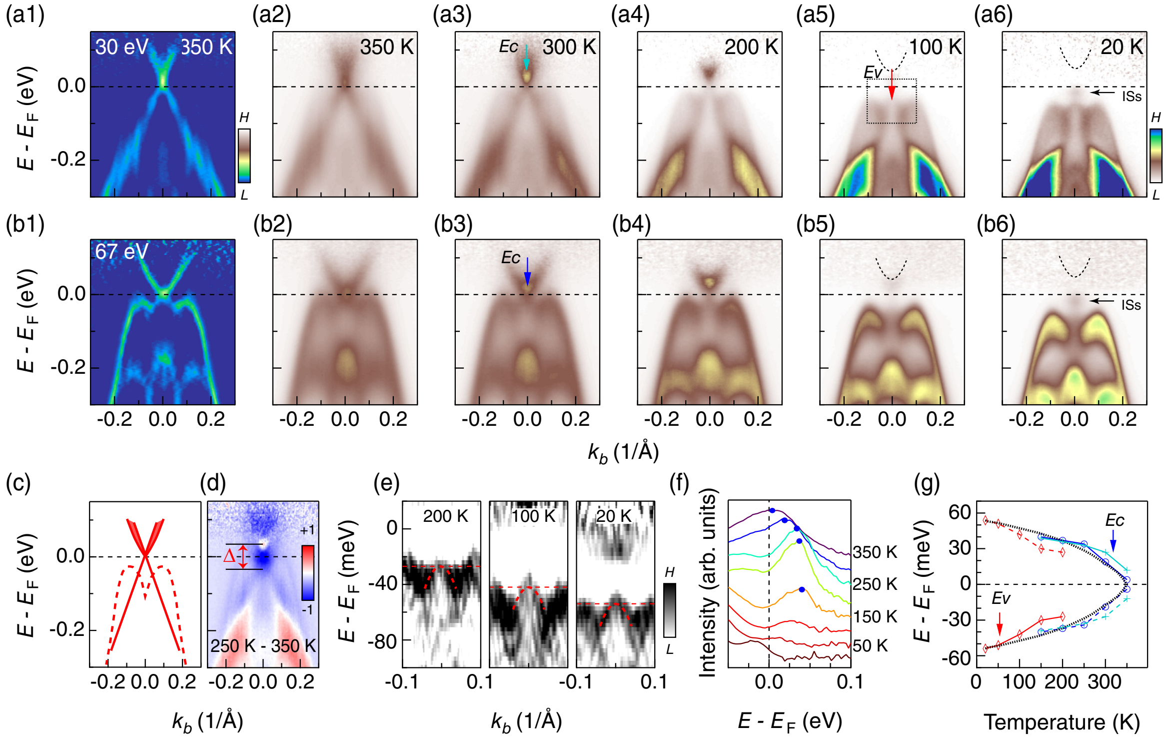

FIG. 2. Temperature evolution of the band structure and energy gap in $Ta_2Pd_3Te_5$. (a1) The curvature plot of (a2). (a2)–(a6) The electronic structure along the chain direction at $k_c = 0$ measured by ARPES from 350 to 20 K with 30-eV photons. (b1) The curvature plot of (b2). (b2)–(b6) The same data as (a2)–(a6) but measured with 67-eV photons. The black dashed lines in (a5) and (a6) and (b5) and (b6) sketch the conduction band above E_F. The black arrows in (a6) and (b6) mark the in-gap impurity states (ISs), which do not cross the Fermi level [see their high-resolution EDCs in Fig. 5(d)]. The details of impurity states are discussed in Fig. 5. All data are divided by the Fermi function at measured temperatures to remove the cutoff effect above E_F. (c) Sketch of band dispersions extracted from 30- and 67-eV data. The cone-shaped bands crossing E_F and the m-shaped band not crossing E_F are represented by solid and dashed lines, respectively. The conduction bands from 30- and 67-eV data have slightly different dispersions. (d) Intensity difference between 250 and 350 K data measured with 30-eV photons. The blue area around E_F indicates the opening of the energy gap Δ. (e) EDC curvature plot for the 30-eV data enlarging the valence-band top [dashed box in (a5)] for three different temperatures (200, 100, and 20 K). The valence-band top [red arrow in (a5)] is extracted from the curvature-enhanced dispersion. (f) EDCs of the conduction band at $k_b = k_c = 0$ extracted from 67-eV data for different temperatures. The blue dots indicate the conduction-band bottom [blue arrow in (b3)]. (g) Temperature dependence of the valence-band top (E_v) and conduction-band bottom (E_c) demonstrating the gap evolution. The E_v (solid red line) is extracted from (e), and E_c (solid blue line) is extracted from (f). The E_c curve in cyan color is extracted from EDCs in 30-eV data in (a). As both E_c and E_v values are acquired at 150 and 200 K and they are roughly equal, it is reasonable to assume that the band gap opens symmetrically to E_F. Then we get the full temperature evolution of the conduction and valence bands by mirroring the blue, cyan, and red lines. The entire evolution of the gap with the temperature is illustrated by the dashed black lines.

temperature. From this result, we conclude that the gap has a value of approximately 100 meV at 20 K, and closes at about 350 K.

As a comparison, we further measure the band structure of $Ta_2Ni_3Te_5$, which has the same crystal structure as $Ta_2Pd_3Te_5$. At low temperature 10 K [Fig. 3(d)], the band structure of $Ta_2Ni_3Te_5$ also shows an m-shaped band [red line in Fig. 3(d)] and a parabolic band [blue line in Fig. 3(d)] near E_F, similar to the one in Fig. 1(g). In sharp contrast to the spontaneous gap opening in $Ta_2Pd_3Te_5$, we notice the valence band in $Ta_2Ni_3Te_5$ does not shift with the temperature at all, as shown in Figs. 3(a)–3(d) and their curvature plot Figs. 3(e)–3(h). The valence-band dispersion at 10 K is extracted from EDC peaks in Fig. 3(h) and plotted in both Figs. 3(e) and 3(h). We find the dispersion from 10 K overlaps with the 300 K data very well, indicating the valence band has no change from 300 to 10 K. The EDCs at $k_b = 0$ at different temperatures are plotted in Fig. 3(i). As guided by the red dashed line in Fig. 3(i), the EDC peaks show no change over a temperature range of 10–300 K. We also extract the EDC peaks in Figs. 3(e)–3(h) and plot the peak position with a blue line in Fig. 3(j). The curve is almost flat, further demonstrating the absence of energy gap change. $Ta_2Ni_3Te_5$ is a semiconductor, while $Ta_2Pd_3Te_5$ is a semimetal at 350 K. At the same time, the spontaneous gap opening is absent in $Ta_2Ni_3Te_5$ but exists in $Ta_2Pd_3Te_5$. Since the two materials have exactly the same crystal structure, we conclude that the spontaneous gap opening with the temperature is originated from the semimetal nature of $Ta_2Pd_3Te_5$, and

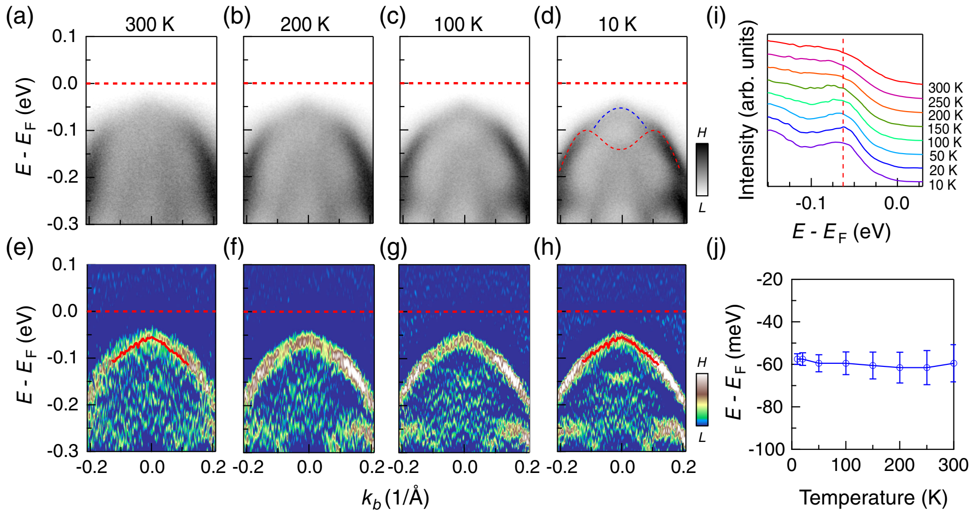

FIG. 3. Temperature evolution of the band structure in $Ta_2Ni_3Te_5$. (a)–(d) The electronic structure along the chain direction at $k_c = 0$ measured from 300 to 10 K with 7-eV photons. (e)–(h) The curvature plot of (a)–(d). The red lines in (e) and (h) are the same curve, which is extracted from EDC peaks in (h). (i) Evolution of EDCs with temperature at $k_b = 0$. (j) Shift of valence-band top with temperature. Blue dots are extracted from EDC peaks in (e)–(h).

it is not a simple conduction-band and valence-band shift with the temperature as in some semiconductors [34–36].

To distinguish the origin of the spontaneous gap opening in $Ta_2Pd_3Te_5$, we deposit potassium on the sample surface to dope extra carriers and investigate how the gap evolves. Figures 4(a) and 4(b) show the ARPES dispersions and their curvature intensities, respectively, measured at 10 K after deposition for different times from zero up to four minutes (from left to right panels). The most pronounced variation is seen in the conduction band; its bottom shifts down below E_F after a 0.5-minute deposition. With further deposition, another conduction band at higher energies appears below E_F. The appearance of these conduction bands can also be identified in the momentum distribution curves (MDCs) at E_F [Fig. 4(c)]. From the MDC maxima, we determine the conduction band near E_F for one-, two- and four-minute doping, and display these by red dots in Fig. 4(b). To analyze the conduction-band shift quantitatively, we fit each result to a parabolic function [solid red lines in Fig. 4(b)]. In the fitting procedure, the quadratic term is fixed since carrier doping should not renormalize the band. We estimate the conduction-band bottom from the fitting curves and plot it against the deposition time in Fig. 4(d) by red dots.

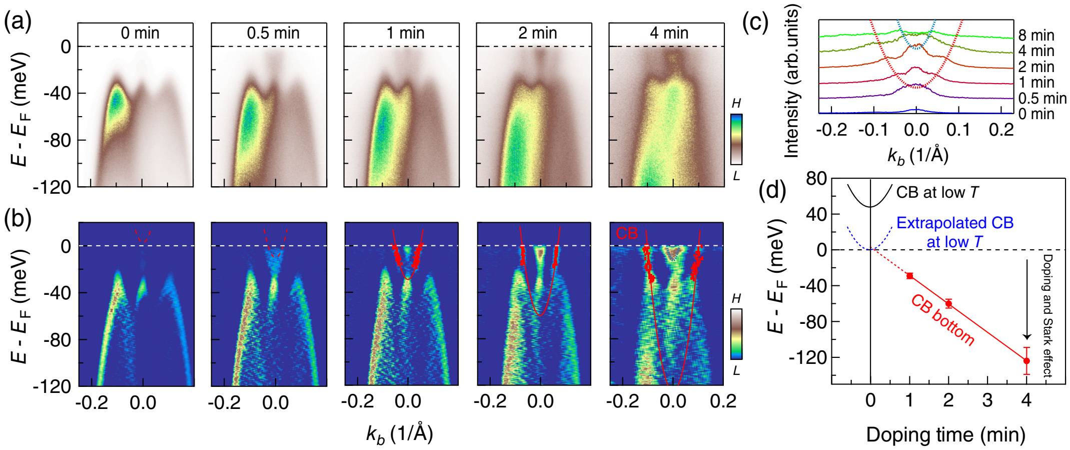

FIG. 4. Effect of potassium deposition on the band structure of $Ta_2Pd_3Te_5$. (a) Evolution of the band structure along the chain direction at $k_c = 0$ with potassium deposition taken at 10 K. (b) Curvature intensity plot of (a). The energy states (small red dots) near E_F in one-, two- and four-minute data are extracted from the peak positions of MDCs. The red lines are parabolic fits to the red dots. (c) Variations of MDCs at E_F with the time of potassium deposition. Dashed lines illustrate the change of the Fermi vector k_F of the conduction bands. (d) Evolution of the conduction band (CB) with potassium deposition. The red dots represent the band bottom of the fitted bands in (b). The solid red line is a linear fit to the red dots, and the dashed red line is the extrapolation of it to zero minutes.

The potassium deposition introduces not only extra carriers but also the Stark effect due to the electric field induced by the ionized potassium adatoms at the surface. Whereas the carrier doping shifts the conduction and valence bands both to higher binding energies, the Stark effect shifts these bands in opposite energy directions to each other [37–41]. That is why, in our data, the conduction band shifts down and eventually overlaps with the valence band at larger potassium deposition. The shift of the conduction band is confirmed to have a linear behavior with deposition time, as shown by the fitted solid red line in Fig. 4(d). This implies that the carrier doping and Stark effect both change the band position linearly for energy. Extrapolation of the conduction-band bottom to zero minutes should remove these linear shifts from the carrier doping and Stark effect and recover the original band position [41]. However, we find that the bottom of the extrapolated conduction band [blue dashed curve in Fig. 4(d)] does not coincide with that of the original band at 10 K [black solid curve in Fig. 4(d)], which is about 50 meV above E_F. Instead, the extrapolated conduction-band bottom almost touches E_F. This indicates that there is a third effect that moves down the conduction band at low deposition (<1 min), except for the carrier doping and Stark effect, which are dominant at high deposition (>1 min). Since the extrapolated conduction-band bottom locates at the energy position the same as the conduction-band bottom in the gapless high-temperature phase (350 K), the third effect seems to close the energy gap. Therefore, we conclude that the energy gap is fragile to carrier doping.

By closely investigating the data measured by high-resolution laser-based ARPES, we find double flat bands near E_F within the energy gap at 10 K. The in-gap flat bands have relatively low spectral intensities, and these are observed only with the light of proper polarization. In Figs. 5(a) and 5(c), we exhibit the ARPES images capturing these flat-band signals perpendicular to and parallel to the 1D chains, respectively. The flat bands are clearly visible, although the color contrast needs to be changed till saturating the intensities of the valence band. The spectral weight for the in-gap flat bands modulates along the momentum axis [Fig. 5(a)]. This modulation coincides with the momentum variation of the valence-band intensity due to the matrix element effect; it is, indeed, removed by normalizing the EDCs to the intensities of the valence band [Fig. 5(b)], which indicates the in-gap flat bands have a close relation with the valence band. The EDCs of the flat bands are displayed in Fig. 5(d). Here, the spectra are integrated over the momentum regions marked by arrows in Figs. 5(a) and 5(c). The flat bands are located at approximately −8 and −18 meV in these data and appear only when using s- and p-polarized light for the data taken perpendicular to and parallel to the chain direction, respectively.

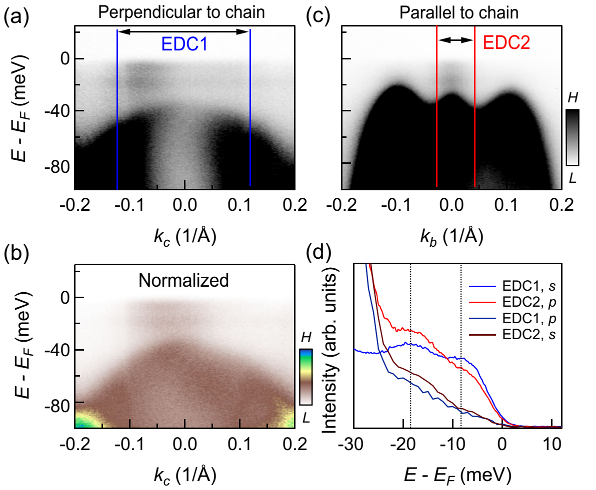

FIG. 5. Observation of double flat bands inside the energy gap in $Ta_2Pd_3Te_5$. (a) Band structure observed perpendicular to the chain direction at $k_b = 0$ measured at 10 K with s-polarized light. To enhance the visibility of in-gap states, the color scale is adjusted to saturate the intensities of valence bands. (b) The same data as (a) but normalized to the intensities of the valence band to remove the matrix element effect. (c) Band structure observed along the chain direction at $k_c = 0$ measured at 10 K with p-polarized light. (d) EDCs focusing on the in-gap flat bands. EDC 1 and EDC 2 are integrated over momentum regions indicated by the arrows in (a) and (c), respectively. These EDCs are measured with both s- and p-polarized light. The dashed lines mark peak energies of about −8 and −18 meV.

We note here that these flat bands are relatively weak in intensity but far enough from E_F, as is clear from the EDCs in Fig. 5(d), so that they are not a residual part of a conduction band cut off by the Fermi function, such as polaronic bands [42–44]. The in-gap flat bands generally come from random impurities or defects in materials [26,27,45–48]. We notice that the large-scale topographic image of scanning tunneling microscopy shows a reasonable amount of defects in $Ta_2Pd_3Te_5$ [30]. The M-H and susceptibility measurements for our samples (Supplemental Material [32] Fig. 10) show no evidence of magnetic order. By fitting a curve of the paramagnetic susceptibility to the data, we get a magnetic moment per atom to be about $0.03\mu_B$. This value is small enough to conclude that the impurities or defects do not have a large magnetic moment and should be nonmagnetic. We also measure crystals synthesized by a different method and detect similar but more intense signals of the in-gap states, where the temperature dependence of the in-gap states also suggests an impurity origin (see Supplemental Material [32] Fig. 7 for more details). In a simple two-band model with local impurity scattering, only one flat band of impurity states exists, either below the conduction band or above the valence band. However, if the conduction and valence bands are hybridized when the gap opens, it is possible to generate double impurity bands inside the gap [49,50].

For example, in superconductors, the impurity states appear in a pair inside the superconducting gap due to the particle-hole mixing [27]. Similarly, the double in-gap impurity bands observed in our data suggest that the conduction and valence bands are mixed when the energy gap opens.

The above results on the energy gap can be summarized in the following four points: (i) The gap opens at 350 K from an ideal Dirac semimetal state, and it is associated with a tiny lattice distortion. (ii) The gap opening is absent in a similar material $Ta_2Ni_3Te_5$. (iii) Potassium deposition destroys the energy gap. (iv) Double in-gap impurity bands are observed, suggesting that the conduction band and valence band are hybridized when the gap opens. Some interactions involving electrons may cause the opening or enlarging of a band gap (namely, "interaction-induced gap or pseudo-gap"). For example, electron scattering can yield a gaplike feature [51], and electron-phonon coupling can cause a gap size change with the temperature in semiconductors [35,52]. However, an interaction-induced gap or pseudo-gap should not be accompanied by a lattice distortion, should not be fragile to potassium deposition, and should not lead to double impurity states. The spontaneous gap opening we observed in $Ta_2Pd_3Te_5$ is most likely induced by an ordered state (namely, "order-induced gap"). For example, CDW, spin-density-wave (SDW), superconductivity, and excitonic states all generate an electronic energy gap when the order appears. Among electronic orders, we exclude the possibility of superconductivity by resistivity measurement. Density-wave states (CDW or SDW) cannot be a candidate either, since the Fermi surface exists only around $k = 0$, having no chance to form density waves with a finite wave vector Q.

An excitonic order matches the observed results in a perfect way. First of all, $Ta_2Pd_3Te_5$ is an almost ideal Dirac semimetal. The carrier density is almost zero, and the electron and hole excitations are almost symmetric. Therefore, the screening of the Coulomb interaction is very weak, and the electrons and holes can be easily bounded by long-range Coulomb interaction, of which the binding energy is clearly larger than the semimetal gap (0 eV). Thus, an excitonic order could naturally occur. More importantly, all four observations mentioned above on the energy gap from (i) to (iv) can be explained well by excitonic states: (i) The excitonic gap has a similar temperature dependence to that of a superconductor or a CDW or SDW. When the excitonic order forms, the electron-phonon coupling leads to the tiny lattice distortion. (ii) $Ta_2Pd_3Te_5$ has an ideal Dirac-type band. Such a band structure is very unstable against excitonic order, so it is natural to have excitonic order in $Ta_2Pd_3Te_5$ and no such order in semiconducting $Ta_2Ni_3Te_5$. (iii) When extra carriers are doped, the electron-hole balance could be destroyed, and the binding of excitons becomes weak, reducing the excitonic gap in $Ta_2Pd_3Te_5$. Note that such a technique—doping carriers by potassium to destroy the excitonic gap—has been widely used to prove the existence of excitonic states [12,40,41]. (iv) According to calculations, double flat bands of in-gap impurity states should appear in excitonic insulators with nonmagnetic impurities [2,49,50]. All these arguments lead us to conclude that an excitonic order is the most likely mechanism for the energy gap in $Ta_2Pd_3Te_5$. In the previous excitonic candidate Ta_2NiSe_5, there is an obvious structure transition when the gap opens, which leads to the debate whether the gap is originated from structure transition or from excitonic order. In $Ta_2Pd_3Te_5$, the lattice distortion is very tiny and even undetectable by XRD and specific heat measurements (see Supplemental Material [32] Fig. 2). It is unlikely to produce the observed large gap from such a tiny lattice distortion. The spontaneous gap opening should come from the excitonic order, and the tiny lattice distortion is a secondary phenomenon from the excitonic order. We note that another paper [55] also observed evidences for an excitonic order in $Ta_2Pd_3Te_5$ at the same time.

An ordered state expects a jump in specific heat at the critical temperature. However, no jump was distinguished in our specific heat measurement at the gap-opening temperature (350 K), as shown in Supplemental Material [32] Fig. 2. We note that a pure electronic transition at high temperature should not be judged from the specific heat jump, as electronic specific heat at high temperature is too small compared to the lattice specific heat. For example, the electronic heat capacity constant of iron, a typical metal, is $\gamma = 4.98\ \mathrm{mJ/(mol\,K^2)}$ [53], and the electronic heat capacity at 350 K is estimated to be $C_e = \gamma T = 1.7\ \mathrm{J/mol\,K}$. On the other hand, a total heat capacity of $Ta_2Pd_3Te_5$ is obtained as about 250 J/mol K at 350 K from our measurement (Supplemental Material [32] Fig. 2). A simple calculation tells us that the electronic heat capacity is 2 orders smaller than the lattice heat capacity: $1.7/(250\text{–}1.7) \ll 0.01$. In particular, $Ta_2Pd_3Te_5$ is an ideal Dirac semimetal with almost zero carrier density; thus, the electronic heat capacity must be even much smaller than that of a typical metal (for example, the electronic heat capacity of semimetallic bismuth is more than 100 times smaller than that of iron [53]). Therefore, even if there is a jump induced by electronic order, it would be too small to be distinguished at 350 K. Interestingly, this situation is similar in superconductors: The specific heat jump for superconducting transition in some cuprates is not distinguished with T_c around or higher than 100 K [54]. On the other hand, although there is a lattice distortion accompanied by the excitonic transition resolved by electron diffraction, it is very tiny and likely does not produce an observable specific heat jump either, which we discussed previously.

The previous excitonic insulator candidates $TiSe_2$ and Ta_2NiSe_5 coexist with either a CDW or structure transition [13,17]. The coexistence of different phases makes it difficult to justify excitonic states. In contrast, there is no entangling order in $Ta_2Pd_3Te_5$. The lattice distortion observed in electron diffraction is too tiny and should be a consequence of the excitonic order. Although further experimental evidence would be desired to reach a definitive conclusion, our results provide that quasi-1D $Ta_2Pd_3Te_5$ is the first promising candidate of an excitonic insulator in which entangled phases are absent, being highly advantageous for developing the condensed matter physics on excitonic states.

We thank J. X. Li, H. J. Zhang, W. Chen, Z. Zhu, X. X. Wu, Q. H. Wang, S. Bao, J. S. Wen, and J. R. Huang for useful discussions and support. This work was supported by the National Natural Science Foundation of China (Grants No. 12274209, No. U2032204, No. 12188101, No. 11504329, No. 92065203, and No. 12174430), the Ministry of Science and Technology of China (Grant No. 2022YFA1403800), the Informatization Plan of Chinese Academy of Sciences (Grant No. CAS-WX2021SF-0102), the Strategic Priority Research Program of Chinese Academy of Sciences (Grant No. XDB33000000), the China Postdoctoral Science Foundation funded project (Grant No. 2021M703461), the Center for Materials Genome, the Beijing Natural Science Foundation (Grant No. JQ23022), the Beijing Nova Program (Grant No. Z211100002121144), Zhejiang Provincial Natural Science Foundation of China (Grant No. LZ23A040002), National Key R&D Program of China (Grant No. 2022YFA1402502), the JSPS KAKENHI (Grants No. JP18H01165, No. JP19H00651, No. JP21H04439 and No. JP23K17351), JST ERATO-FS (Grant No. JPMJER2105), MEXT Q-LEAP (Grant No. JPMXS0118068681), MEXT under the "Program for Promoting Researches on the Supercomputer Fugaku" (Basic Science for Emergence and Functionality in Quantum Matter Innovative Strongly Correlated Electron Science by Integration of "Fugaku" and Frontier Experiments, Grant No. JPMXP1020200104) (Project ID No. hp220166), the Asahi Glass Foundation, and the Murata Science Foundation. Use of the Stanford Synchrotron Radiation Lightsource, SLAC National Accelerator Laboratory, is supported by the U.S. Department of Energy, Office of Science, Office of Basic Energy Sciences under Contract No. DE-AC02-76SF00515.

[1] D. Jérome, T. M. Rice, and W. Kohn, *Excitonic insulator*, Phys. Rev. **158**, 462 (1967).
[2] J. Zittartz, *Theory of the excitonic insulator in the presence of normal impurities*, Phys. Rev. **164**, 575 (1967).
[3] J. P. Eisenstein and A. H. MacDonald, *Bose-Einstein condensation of excitons in bilayer electron systems*, Nature (London) **432**, 691 (2004).
[4] L. Du *et al.*, *Evidence for a topological excitonic insulator in* InAs/GaSb *bilayers*, Nat. Commun. **8**, 1971 (2017).
[5] J. I. A. Li, T. Taniguchi, K. Watanabe, J. Hone, and C. R. Dean, *Excitonic superfluid phase in double bilayer graphene*, Nat. Phys. **13**, 751 (2017).
[6] L. Ma, P. X. Nguyen, Z. Wang, Y. Zeng, K. Watanabe, T. Taniguchi, A. H. MacDonald, K. F. Mak, and J. Shan, *Strongly correlated excitonic insulator in atomic double layers*, Nature (London) **598**, 585 (2021).
[7] X. Liu, J. I. A. Li, K. Watanabe, T. Taniguchi, J. Hone, B. I. Halperin, P. Kim, and C. R. Dean, *Crossover between strongly coupled and weakly coupled exciton superfluids*, Science **375**, 205 (2022).
[8] R. Wang, T. A. Sedrakyan, B. Wang, L. Du, and R.-R. Du, *Excitonic topological order in imbalanced electron-hole bilayers*, Nature (London) **619**, 57 (2023).
[9] Y. Jia *et al.*, *Evidence for a monolayer excitonic insulator*, Nat. Phys. **18**, 87 (2022).
[10] B. Sun *et al.*, *Evidence for equilibrium exciton condensation in monolayer* WTe_2, Nat. Phys. **18**, 94 (2022).
[11] Q. Gao, X. Lyu, T. Tong, A. I. Lim, T. Li, J. Bao, and Y. H. Hu, *Evidence of high-temperature exciton condensation in a two-dimensional semimetal*, Nat. Commun. **14**, 994 (2023).
[12] Y. Song *et al.*, *Signatures of the exciton gas phase and its condensation in monolayer* 1T-$ZrTe_2$, Nat. Commun. **14**, 1116 (2023).
[13] H. Cercellier *et al.*, *Evidence for an excitonic insulator phase in* 1T-$TiSe_2$, Phys. Rev. Lett. **99**, 146403 (2007).
[14] C. Monney *et al.*, *Spontaneous exciton condensation in* 1T-$TiSe_2$*: BCS-like approach*, Phys. Rev. B **79**, 045116 (2009).
[15] C. Monney, C. Battaglia, H. Cercellier, P. Aebi, and H. Beck, *Exciton condensation driving the periodic lattice distortion of* 1T-$TiSe_2$, Phys. Rev. Lett. **106**, 106404 (2011).
[16] A. Kogar *et al.*, *Signatures of exciton condensation in a transition metal dichalcogenide*, Science **358**, 1314 (2017).
[17] Y. Wakisaka *et al.*, *Excitonic insulator state in* Ta_2NiSe_5 *probed by photoemission*, Phys. Rev. Lett. **103**, 026402 (2009).
[18] K. Sugimoto, S. Nishimoto, T. Kaneko, and Y. Ohta, *Strong coupling nature of the excitonic insulator state in* Ta_2NiSe_5, Phys. Rev. Lett. **120**, 247602 (2018).
[19] H. M. Bretscher *et al.*, *Imaging the coherent propagation of collective modes in the excitonic insulator* Ta_2NiSe_5 *at room temperature*, Sci. Adv. **7**, eabd6147 (2021).
[20] K. Fukutani, R. Stania, C. I. Kwon, J. S. Kim, K. J. Kong, J. Kim, and H. W. Yeom, *Detecting photoelectrons from spontaneously formed excitons*, Nat. Phys. **17**, 1024 (2021).
[21] K. Kim, H. Kim, J. Kim, C. Kwon, J. S. Kim, and B. J. Kim, *Direct observation of excitonic instability in* Ta_2NiSe_5, Nat. Commun. **12**, 1969 (2021).
[22] M. D. Watson, I. Marković, E. A. Morales, P. Le Fèvre, M. Merz, A. A. Haghighirad, and P. D. C. King, *Band hybridization at the semimetal-semiconductor transition of* Ta_2NiSe_5 *enabled by mirror-symmetry breaking*, Phys. Rev. Res. **2**, 013236 (2020).
[23] E. Baldini *et al.*, *The spontaneous symmetry breaking in* Ta_2NiSe_5 *is structural in nature*, arXiv:2007.02909v1.
[24] C. Chen *et al.*, *Lattice fluctuation induced pseudogap in quasi-one-dimensional* Ta_2NiSe_5, Phys. Rev. Res. **5**, 043089 (2023).

[25] J. Yao *et al.*, *Excitonic instability in* $Ta_2Pd_3Te_5$, arXiv:2401.01222.

[26] M. I. Salkola, A. V. Balatsky, and J. R. Schrieffer, *Spectral properties of quasiparticle excitations induced by magnetic moments in superconductors*, Phys. Rev. B **55**, 12648 (1997).

[27] A. V. Balatsky, I. Vekhter, and J.-X. Zhu, *Impurity-induced states in conventional and unconventional superconductors*, Rev. Mod. Phys. **78**, 373 (2006).

[28] Z. Guo *et al.*, *Quantum spin Hall effect in* $Ta_2M_3Te_5$ *(*$M = \mathrm{Pd, Ni}$*)*, Phys. Rev. B **103**, 115145 (2021).

[29] N. Higashihara *et al.*, *Superconductivity in* $Nb_2Pd_3Te_5$ *and chemically-doped* $Ta_2Pd_3Te_5$, J. Phys. Soc. Jpn. **90**, 063705 (2021).

[30] X. Wang *et al.*, *Observation of topological edge states in the quantum spin Hall insulator* $Ta_2Pd_3Te_5$, Phys. Rev. B **104**, L241408 (2021).

[31] H.-Q Qiu *et al.*, *Crystal growth and electronic transport property of ternary* Pd*-based tellurides*, Acta Phys. Sin. **71**, 227401 (2022).

[32] See Supplemental Material at http://link.aps.org/supplemental/10.1103/PhysRevX.14.011047 for extra electron diffraction, XRD, specific heat, theory, ARPES, and magnetic susceptibility data.

[33] P. Zhang, P. Richard, T. Qian, Y.-M. Xu, X. Dai, and H. Ding, *A precise method for visualizing dispersive features in image plots*, Rev. Sci. Instrum. **82**, 043712 (2011).

[34] R. Pässler, *Dispersion-related description of temperature dependencies of band gaps in semiconductors*, Phys. Rev. B **66**, 085201 (2002).

[35] F. Giustino, S. G. Louie, and M. L. Cohen, *Electron-phonon renormalization of the direct band gap of diamond*, Phys. Rev. Lett. **105**, 265501 (2010).

[36] Y. Zhang, Z. Wang, J. Xi, and J. Yang, *Temperature-dependent band gaps in several semiconductors: From the role of electron-phonon renormalization*, J. Phys. Condens. Matter **32**, 475503 (2020).

[37] K. H. Khoo, M. S. C. Mazzoni, and S. G. Louie, *Tuning the electronic properties of boron nitride nanotubes with transverse electric fields: A giant dc Stark effect*, Phys. Rev. B **69**, 201401(R) (2004).

[38] A. Ramasubramaniam, D. Naveh, and E. Towe, *Tunable band gaps in bilayer transition-metal dichalcogenides*, Phys. Rev. B **84**, 205325 (2011).

[39] J. Kim, S. S. Baik, S. H. Ryu, Y. Sohn, S. Park, B.-G. Park, J. Denlinger, Y. Yi, H. J. Choi, and K. S. Kim, *Observation of tunable band gap and anisotropic Dirac semimetal state in black phosphorus*, Science **349**, 723 (2015).

[40] K. Fukutani, R. Stania, J. Jung, E. F. Schwier, K. Shimada, C. I. Kwon, J. S. Kim, and H. Woong Yeom, *Electrical tuning of the excitonic insulator ground state of* Ta_2NiSe_5, Phys. Rev. Lett. **123**, 206401 (2019).

[41] L. Chen, T. T. Han, C. Cai, Z. G. Wang, Y. D. Wang, Z. M. Xin, and Y. Zhang, *Doping-controlled transition from excitonic insulator to semimetal in* Ta_2NiSe_5, Phys. Rev. B **102**, 161116(R) (2020).

[42] S. Moser *et al.*, *Tunable polaronic conduction in anatase* TiO_2, Phys. Rev. Lett. **110**, 196403 (2013).

[43] Z. Wang *et al.*, *Tailoring the nature and strength of electron–phonon interactions in the* $SrTiO_3(001)$ *2D electron liquid*, Nat. Mater. **15**, 835 (2016).

[44] G. Antonius, Y.-H. Chan, and S. G. Louie, *Polaron spectral properties in doped* ZnO *and* $SrTiO_3$ *from first principles*, Phys. Rev. Res. **2**, 043296 (2020).

[45] A. V. Balatsky, M. I. Salkola, and A. Rosengren, *Impurity-induced virtual bound states in d-wave superconductors*, Phys. Rev. B **51**, 15547 (1995).

[46] S. H. Pan, E. W. Hudson, K. M. Lang, H. Eisaki, S. Uchida, and J. C. Davis, *Imaging the effects of individual zinc impurity atoms on superconductivity in* $Bi_2Sr_2CaCu_2O_{8+\delta}$, Nature (London) **403**, 746 (2000).

[47] D. Zhang, *Nonmagnetic impurity resonances as a signature of sign-reversal pairing in* FeAs*-based superconductors*, Phys. Rev. Lett. **103**, 186402 (2009).

[48] P. Zhang *et al.*, *Observation of momentum-confined in-gap impurity state in* $Ba_{0.6}K_{0.4}Fe_2As_2$*: Evidence for antiphase* $s_\pm$ *pairing*, Phys. Rev. X **4**, 031001 (2014).

[49] T. Ichinomiya, *Impurity-induced ferromagnetism in a doped triplet excitonic insulator*, Phys. Rev. B **63**, 045113 (2001).

[50] Y. Dubi and A. V. Balatsky, *Impurity-induced bound states and proximity effect in a bilayer exciton condensate*, Phys. Rev. Lett. **104**, 166802 (2010).

[51] S. H. Ryu *et al.*, *Pseudogap in a crystalline insulator doped by disordered metals*, Nature (London) **596**, 68 (2021).

[52] B. Monserrat, *Correlation effects on electron-phonon coupling in semiconductors: Many-body theory along thermal lines*, Phys. Rev. B **93**, 100301(R) (2016).

[53] C. Kittel, *Introduction to Solid State Physics* (Wiley, New York, 2004).

[54] A. Gauzzi *et al.*, *Bulk superconductivity at 84 K in the strongly overdoped regime of cuprates*, Phys. Rev. B **94**, 180509(R) (2016).

[55] J. Huang *et al.*, preceding paper, *Evidence for an excitonic insulator state in* $Ta_2Pd_3Te_5$, Phys. Rev. X **14**, 011046 (2024).